

Viscosity of a nonequilibrium hot and dense QCD drop formed at the LHC

J. R. Alvarado García^{1,†}, P. Fierro², A. Fernández Téllez,¹ and I. Bautista^{1,*}

¹*Facultad de Ciencias Físico Matemáticas, Benemérita Universidad Autónoma de Puebla, 1152, Puebla 72570, México*

²*Instituto de Física Luis Rivera Terrazas, Benemérita Universidad Autónoma de Puebla, (IFUAP), Apartado postal J-48 72570, Puebla, México*



(Received 5 December 2022; accepted 4 November 2023; published 4 December 2023)

We compute the bulk, ζ , and shear, η , viscosity over entropy density, s , for the QCD matter formed in small collision systems at LHC. We consider a scenario of the string percolation model by proposing a global form of the color reduction factor that describes both the thermodynamic limit and its maximum deviation due to small-bounded effects. Our method involves estimations at vanishing baryon-chemical potential, assuming local equilibrium for string clusters in the initial state. To compute η/s , we employed a kinetic approach that accounts QCD states as an ideal gas of partons, while ζ/s is computed by using two different approaches: a simple kinetic formula and the causal dissipative relativistic fluid dynamics formulation. Our results align with lattice QCD computations and Bayesian methods and are consistent with holographic conjecture bounds. Furthermore, our findings support the notion of a strongly interacting medium, similar to that observed in nuclear collisions, albeit with a phase transition occurring outside the thermodynamic limit.

DOI: [10.1103/PhysRevD.108.114002](https://doi.org/10.1103/PhysRevD.108.114002)

I. INTRODUCTION

The string percolation model (SPM) has described successfully the collective effects on medium formed at heavy ion collisions from the Relativistic Heavy Ion Collider (RHIC) to the Large Hadron Collider's (LHC) energies [1–9]. At these energy regimes, nonperturbative QCD takes a major role in describing phenomena through phenomenological models, such as the characteristics of the QCD phase diagram and the phase transition properties, which can be studied in terms of the systems' thermodynamic quantities, transport coefficients, and bulk properties [9]. Recently, to obtain the values of bulk and shear viscosity from nuclear collisions, relativistic hydrodynamics have been used to calculate the temperature dependence of these coefficients [10–15], as well as theoretical limits in AdS/CFT correspondence and holographic link with quark-gluon plasma (QGP) [16,17].

The string percolation model uses the percolation theory for nonperturbative heavy ion physics by utilizing as main objects the effective color sources and describing their physical properties such as color field, momentum, and

multiplicity [8,9]. The functional form of its main parameters was deduced from Monte Carlo simulations considering thermodynamic limit. And, more recently, the results of clustering of color sources that consider finite size, profile distribution function, and the initial geometry effects (which correspond to systems far from the thermodynamic limit, which, from now on, we will denote as nonTL) were studied and compared with what was previously reported for known observables, such as the thermal-like temperature extracted from the transverse momentum spectra and the estimation of thermodynamic quantities [18,19]. In this work, we study from a phenomenological view the signatures of collective effects reported on [20,21]. Specifically, we studied the bulk properties like the modification of the behavior of the speed of sound, and we calculated the bulk viscosity coefficient, which are significant for nonthermal equilibrium systems and highlights the benefits that our approach provides. With this new perspective on the SPM, we can see new light on how the effects of bulk properties weigh on reaching critical temperature on nonTL systems, which is the first step for computing the bulk properties for nonthermal equilibrium systems.

In the following section, we present the basics of the string percolation model. Then, we proceed with exploring the consequences of considering the nonTL scenarios in the SPM framework in Sec. III. In Secs. IV and V, we introduce the temperature and energy density, respectively, as usually reported. Finally, in Secs. VI and VII, we discuss the results

*Corresponding author: irais.bautista@cfm.buap.mx

†j.ricardo.alvarado@cern.ch

Published by the American Physical Society under the terms of the [Creative Commons Attribution 4.0 International license](https://creativecommons.org/licenses/by/4.0/). Further distribution of this work must maintain attribution to the author(s) and the published article's title, journal citation, and DOI. Funded by SCOAP³.

on bulk and shear viscosity to entropy density ratios of TL and nonTL scenarios in the SPM.

II. PERCOLATION COLOR SOURCES

The string percolation model uses percolation theory, which is closely associated with the study of phase transitions and transport phenomena [22–24], necessary to characterize the medium formed in ultrarelativistic heavy ion collisions. The interaction between colliding nuclei is effectively represented by the formation of extended color flux tubes that are stretching among the colliding partons. We consider the projection of the color flux tubes in the transverse plane, from now on, named strings, in order to use the two-dimensional percolation approach, which, unlike in the thermodynamic approaches, is able to describe a phase transition without defining a temperature in a thermodynamic equilibrium [8,9].

The strings can be seen as small disks characterized by their transverse area, which is on average taken as $S_0 = \pi r_0^2$ (~ 3.5 mb from the parton-parton cross section of bilocal correlation functions [25,26] and r_0 the radius of a single disk).

The percolation approach is only used to characterize the string density in the initial state. Based on the initial density, this approach gives the probability of forming a spanning color strings system, which means that in a two-dimensional percolation approach, a geometrical connected system of disks represents a connected color flux tubes state. The spanning system will then later evolve due to the Schwinger mechanism where a temperature is defined as the corresponding thermal T slope of p_T -exponential momentum distribution. In this sense, the temperature is associated with the final state of experimental observations as we will detail in Sec. IV.

For characterizing the system, an order parameter is introduced, which depends on the area fraction occupied by a determined number of strings:

$$\xi = \frac{S_0}{S} N_s, \quad (1)$$

where N_s is the number of initial strings in an event, which, for a minimum bias distribution, escalates with energy as a power law [27]:

$$N_s = 2 + 4 \frac{S_0}{S} \left(\frac{\sqrt{s}}{m_p} \right)^{2\lambda}, \quad (2)$$

with m_p the proton mass and $\lambda = 0.196 \pm 0.005$ a fit parameter shown in Fig. 1. For a large number of strings in an event, it is required to have a large number of partonic interactions that can be achieved at high collision energies or a large number of colliding partons, like AA collisions. The created disk's distribution and overlapping (cluster

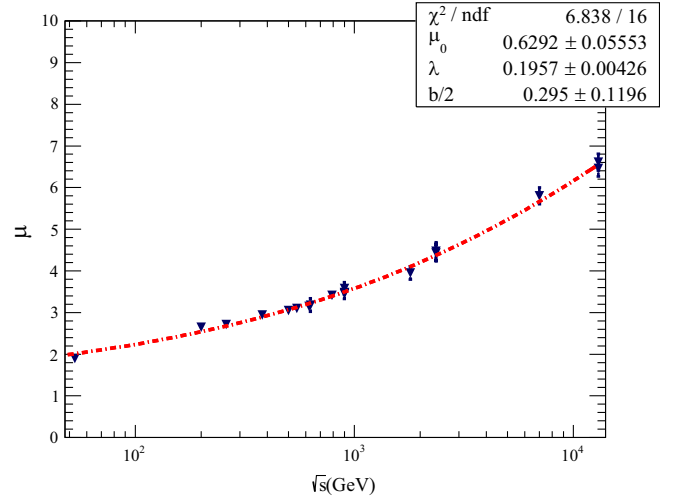


FIG. 1. Fit over experimental data for multiplicity measured on pp collisions from 53 MeV to 13 TeV, data taken from Refs. [29–37].

formation) marks a phase transition when the system starts to percolate for a critical value of the string density ξ_c [9], which depends on the characteristics of the system [28].

In pp , collisions the areas S and S_0 can be described in terms of the radii $r_0 \simeq 0.2385$ fm [38–41] and $R_p \simeq 1$ fm (the radius of a proton). However, to have a more precise description of the overlapping area, we define it as an ellipse in terms of an effective impact parameter b :

$$S = \pi \left(R_p - \frac{b}{2} \right) \sqrt{R_p^2 - \left(\frac{b}{2} \right)^2}. \quad (3)$$

For greatly overlapped areas, we can approximate Eq. (3) as the area of a circle $S \simeq \pi R_p^2$.

Cluster formation implies the creation of new color sources in which color fields are the vector sum of the overlapped areas' color fields. Due to the random orientation of the color fields, the mixed terms vanish. Thus, the color field intensity is proportional to the squared color charges of the original strings \sqrt{n} , and, in consequence, multiplicity μ is

$$\frac{\mu}{\mu_0} = \frac{\langle \sqrt{n} \rangle}{S_0} S = N \frac{\langle \sqrt{n} \rangle}{\xi}, \quad (4)$$

where μ_0 is the multiplicity of a single string [8,9]. So, the number of charged particles generated in the midrapidity region is directly proportional to the initial number of strings of the system [27]:

$$\mu = \mu_0 F(\xi) N_s, \quad (5)$$

where $\mu_0 \sim 0.63$ is calculated from fit over data [29–37], shown in Fig. 1.

From the above equation, a geometric scaling function appears, namely the color reduction factor $F(\xi)$, which emerges naturally from cluster formation [8,9]. This function increases with the string tension of the cluster and the average momentum fraction of the partons $\langle p_T^2 \rangle$. In the thermodynamic limit, $F(\xi)$ depends on the string density ξ as [8,9,42]:

$$F(\xi) = \sqrt{\frac{1 - e^{-\xi}}{\xi}}. \quad (6)$$

This geometric scaling function describes the universality of the scaling law of the system, in correspondence to heavy nuclei.

III. NONTHERMODYNAMIC LIMIT COLOR REDUCTION FACTOR

In the field of heavy-ion collisions, understanding the behavior of small collision systems is of paramount importance. Traditional studies often make predictions for these systems by obtaining $F(\xi)$ by fitting experimental measurements and assuming TL [27,43–45]. While useful, this approach may not be the best method for describing systems far from reaching the TL. To address this, we consider the impact of system size effects [46] and other initial state conditions [18,19,47].

To account for maximum deviations from the TL in $F(\xi)$, we propose a universal function for the color reduction factor that includes an additional damping term. This function captures the TL limit and fits deviations from the geometric scaling function as revealed in simulation results that consider small-bounded effects. This factorization can be expressed as:

$$F_s(\xi) = m \sqrt{\frac{1 - \exp(-\xi)}{\xi}} + c \sqrt{\frac{1 + \exp(-\xi)}{\xi}}, \quad (7)$$

where $m = 0.7714731 \pm 0.01468$ is the weight parameter of the TL contribution to $F(\xi)$ (the typical percolation model), and $c = 0.0609589 \pm 0.007527$ is the weight parameter of the deviation from the nonTL in the percolating system. The difference $\Delta F = F(\xi) - F_s(\xi)$ represents the strength of the fluctuations of the percolating object's properties. The equation reduces to Eq. (6) when $c = 0$ (indicating no additional damping from finite size effects) and $m = 1$ (representing the TL).

This new formulation allows a larger suppression effect above critical string density, which is significant even when c is small due to the large deviation from TL exhibited by the area covered by disks included in our fit [19]. It also explains similar deviations reported for regions just below the critical string density [44,48].

With this improvement to the SPM, we can now better account for effects in a broader range of multiplicity experimental data [36,49–56] and improve the model's predictions for transport coefficients and bulk properties for temperature regions below the critical temperature for nonTL systems. We will demonstrate these improvements in subsequent sections.

We also estimated the effective region of $F_s(\xi)$ for systems that lie between the TL and nonTL using a linear interpolation method. For the derived model-dependent observables, the effective region was calculated through an uncertainty propagation method.

IV. THERMAL DISTRIBUTION

As mentioned before, the local effective thermodynamic quantities are connected with the geometrical properties of the percolating system through $F_s(\xi)$. The string density rules the cluster distribution, and in consequence, the behavior of all thermodynamic quantities, such as temperature that involves the Schwinger mechanism for non-massive particles, on which the strings with higher tension x will break producing $q\bar{q}$ and $qq - \bar{q}\bar{q}$ pairs, which, later on, will combine producing the final state hadrons.

So, the transverse momentum distribution of charged particles is given by [57]:

$$\frac{dN}{dp_T^2} \sim \exp\left(-\pi \frac{p_T^2}{x^2}\right). \quad (8)$$

The tension of the string x^2 fluctuates around its mean value, $\langle x^2 \rangle$, describing a Gaussian distribution of the fluctuations, which convolutes with (8) giving a thermal-like distribution characterized by the mean transverse momentum of a single string $\langle p_T^2 \rangle_0 = \langle x^2 \rangle F_s(\xi) / \pi$ [9,38]:

$$\frac{dN}{dp_T^2} \sim \exp\left(-p_T \sqrt{\frac{2F_s(\xi)}{\langle p_T^2 \rangle_0}}\right), \quad (9)$$

from where we estimate the temperature in the same way as in the Boltzmann distribution:

$$T(\xi) = \sqrt{\frac{\langle p_T^2 \rangle_0}{2F_s(\xi)}}. \quad (10)$$

The critical string density depends on the system's characteristics [18,19,47]. We consider the critical temperature in terms of critical string density $\xi_c = 1.128$ [58] in the same way as [27,59], where $T_c = T(\xi_c)$ so that in TL:

$$\frac{T}{T_c} = \sqrt{\frac{F(\xi_c)}{F(\xi)}} = \frac{0.879947816}{\sqrt{F(\xi)}}. \quad (11)$$

Furthermore, we also see a shift in the critical temperature, now reached at lower ξ for $F_s(\xi)$. We consider the

critical temperature $T_c = 154 \pm 9$ [60], and its respective deviations with ξ to estimate an effective area of the observables as a function of T/T_c .

V. ENERGY DENSITY

In the Stephan-Boltzmann approximation, quarks and gluons are assumed to be noninteracting and massless [61]. The energy density ε is an order parameter in the phase transition from the hadron gas (HG) to QGP, revealing an increment in the internal degrees of freedom. Moreover, the string density ξ is the local order parameter in the SPM that marks the geometric phase transition [9]. In references [9,62,63], energy density from the Bjorken boost invariant 1D hydrodynamics formula [64] is found to be proportional to ξ . Considering that each initial state string can be interpreted as the extended fields among the interacting partons, which has a direct contribution to energy density. This key idea holds for small collision systems [27,43]. Consequently, we use the following relation to estimate energy density:

$$\varepsilon = \zeta \xi, \quad (12)$$

where we found in the same way as [62] that $\zeta = \varepsilon_c / \xi_c = 0.5601 \text{ GeV}/\text{fm}^3$ and see a shift in the critical temperature $T_c(F_s)/T_c(F) = 1.096$ with respect to the TL scenario.

As we can see in Fig. 2, the behavior of the energy density over T^4 as a function of T/T_c agrees with lattice's calculations using staggered fermion actions p4 and asqtad [65]. The observed increment of energy density is related to a rise in the number of degrees of freedom from the hadron-gas phase where there are fewer than in the QGP phase, and

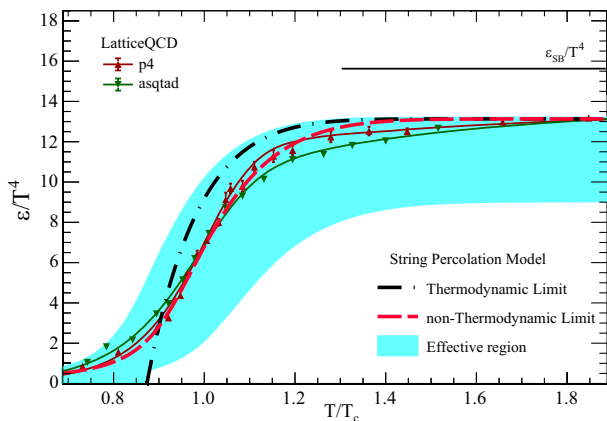


FIG. 2. Energy density over T^4 behavior with respect to T/T_c . The cyan area shows the effective region estimated with ΔF . The red dashed line shows the energy density computed in nonTL, while the black dotted-dashed line is the TL. [9]. We include a comparison with lattice QCD computations p4 (maroon triangles) and asqtad (green triangles) actions with their respective parametrization (continuum lines) [65].

the quantum color numbers contribute to the energy density [66].

VI. SHEAR VISCOSITY

The observable behavior of the elliptic flow suggests that matter created in AA collisions behaves as a near-perfect fluid with a very low viscosity over entropy density ratio [67–75]. It was proposed the indirect measurement of the shear viscosity over entropy density as a probe of the viscosity of the medium created in the collision. More recently, this probe has shown signs of a strongly interacting medium in small collision systems as well [76–80].

Assuming a simple kinetic model of an ideal gas of partons, it is possible to estimate the transport coefficients not in thermodynamic equilibrium, considering that the medium expands as a function of the initial state properties, as was initially proposed in [62].

For computing the ratio of shear viscosity over entropy density η/s in terms of the SPM parameters, we considered the relation given by the relativistic kinetic theory [81], which was also previously used for small collision systems [27,43]:

$$\frac{\eta}{s} = \frac{T\lambda}{5}, \quad (13)$$

where $\lambda = 1/(n\sigma_{tr})$ is the mean free path, with n the number density of an ideal gas of partons and σ_{tr} the transport cross section of its constituents. The number density is directly extracted from the initial number of strings damped by $F_s(\xi)$, which gives the collective medium effects:

$$n = \frac{N_s F_s(\xi)}{SL}, \quad (14)$$

where $L \sim 1 \text{ fm}$ represents the size that a string takes when extended in the beam axis direction. It is worth mentioning that this length has been taken as a first approximation, given that the calculations suggest that this value is in between 0.37 fm and 1.2 fm [82]. On the other hand, we are considering that this formulation takes into account properties of the initial state, which is characterized by its corresponding two-dimensional percolating system, with N_s and S as defined in Sec. II. In the same way, the transport cross section is given by $\sigma_{tr} = S_0 F_s(\xi)$, the transverse size of a single string multiplied by $F_s(\xi)$ [62]. This leads us to estimate the mean free path using the definition of the string density from Eq. (1):

$$\lambda = \frac{L}{\xi F_s^2}, \quad (15)$$

where ξF_s^2 is the area covered by color sources, which is $1 - e^{-\xi}$ in the case of TL [19]. Although the kinetic theory

is applicable when the system is in equilibrium, in this case, we consider that a cluster is locally in equilibrium in the initial state for the appropriate validity of Eq. (15). Moreover, the behavior of λ/L is obtained for the complete system. The upper Fig. 3 shows the λ/L as a function of temperature. For the TL case, λ decreases its value around 1 after the critical temperature [62]. This scenario replicates a situation where particle movement is constrained by the effects of a strongly interacting medium, which aligns with what was observed in AA collisions [67–70]. This is in contrast to pp collisions, where the medium does not achieve thermalization and its effects are less pronounced. Nevertheless, a reduction is still observed after the critical temperature region in the nonTL case.

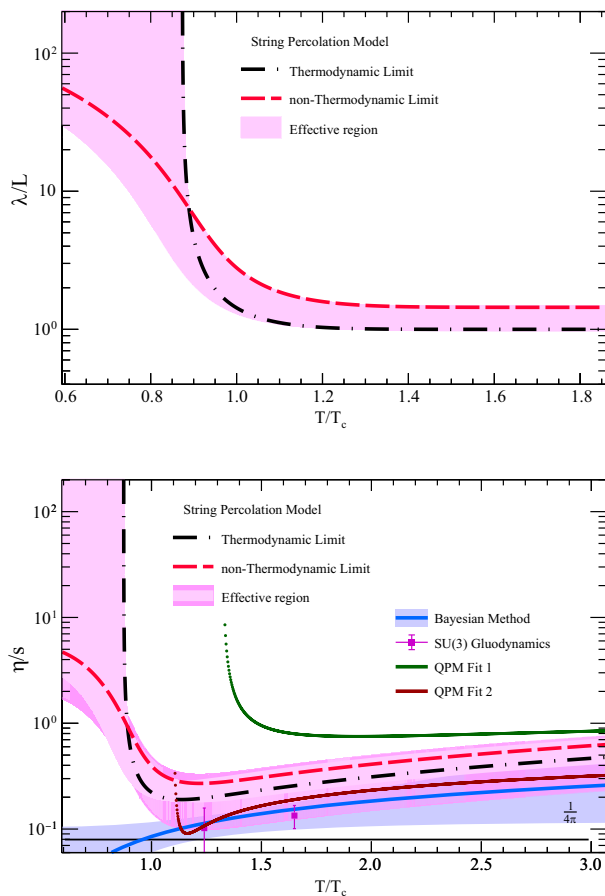


FIG. 3. The (upper figure) mean free path and (lower figure) ratio of shear viscosity over entropy density as a function of T/T_c both calculated on the SPM framework. The red dashed line corresponds to the nonTL computation, while the black dotted-dashed line is the TL one as reported in [27]; the pink area is the estimated effective region, and the magenta in η/s is the extended effective region considering different L size of sources. The results from the Bayesian method [15] are shown in the blue region. The dark magenta squares correspond to SU(3) gauge calculations [83], while the green and red solid lines correspond to QPM fits [84]. The limit of AdS/CFT [16] is included in the black continuum line.

The behavior of λ is inherited in the η/s ratio, where a significant difference between the medium formed in heavy ion collisions and that from small collision systems is shown. The lower Fig. 3 shows a decrease in the η/s ratio, which leads to an enhancement of collectivity effects. The results show that these effects are smaller in pp collisions compared to those estimated for AA collisions. The results on η/s show that its minimum value for TL associated with $F(\xi)$ is reached at $T/T_c = 1.13187$, while the one associated with $F_s(\xi)$ for nonTL is reached at $T/T_c = 1.22508$; the results show an increase in the minimum value of η/s by a factor of 1.4218 from 0.190018 for TL to 0.270179 for nonTL as shown in Fig. 3. These results are compared with the fits for quasiparticle excitations with medium-dependent self-energies (QPM) [84] and the lattice calculation in SU(3) gauge theory [83]. The results from the Bayesian method applied to heavy ion collisions [15] are in between our estimation, and, for $T > T_c$, the conjectured limit of AdS/CFT, $\eta/s \geq 1/(4\pi)$ [16].

Trace anomaly Δ measures the deviation with respect to the conformal behavior and identifies residual interactions in the medium formed [85–87]. It is expected that this observable is related to the medium’s viscosity properties. In previous works, it has been observed qualitatively that the trace anomaly can be approximated as the inverse of shear viscosity over entropy density [59,88]:

$$\Delta \equiv \frac{\epsilon - 3P}{T^4} \simeq \frac{s}{\eta_s}. \quad (16)$$

Trace anomaly as well as the viscosity coefficients are susceptible to QGP phase transition [89]. The behavior of the trace anomaly for nonTL goes accordingly to that

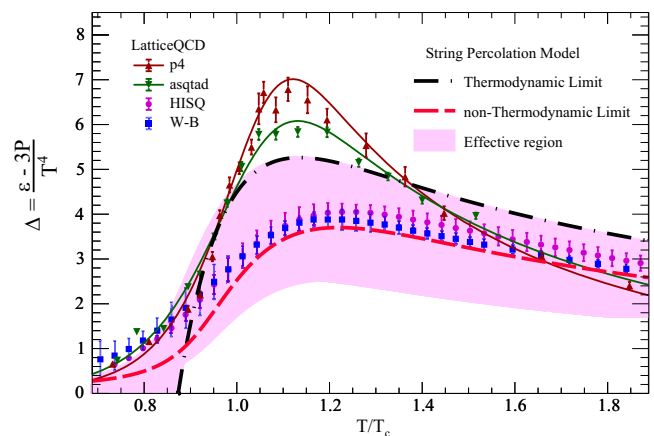


FIG. 4. The behavior of the trace anomaly with respect to T/T_c in TL (black dotted-dashed line) and nonTL (red dashed line) limits and the effective region (pink area) in the SPM framework compare with the results from Lattice QCD p4 (maroon triangles), asqtad (green triangles) [65], HISQ (magenta circles) [91] actions, and the Wuppertal-Budapest Collaboration (W-B) results (blue squares) [90].

reported by Wuppertal-Budapest Collaboration (W-B) using the Symanzik improved gauge and a stout-link improved staggered fermion action [90]. And with the continuum extrapolated results from the HotQCD Collaboration of highly improved staggered quark action [91]. All of these results show a maximum value; for the SPM, this maximum is located at $T/T_c = 1.13621$ in TL and at $T/T_c = 1.21918$ for nonTL (Fig. 4).

Pressure P is obtained from Eq. (16), and from the first law of thermodynamics ($Ts = \varepsilon + P$ [64]), we calculated the entropy density s of the system. The results of $3P/T^4$ and s/T^3 are, respectively, shown in Fig. 5 compared with LQCD [65]. The SPM results agree with those of LQCD. Pressure begins saturation over $3T_c$. For this reason, we can see the less pronounced slope in the decreasing region of trace anomaly after Fig. 4 maximal point.

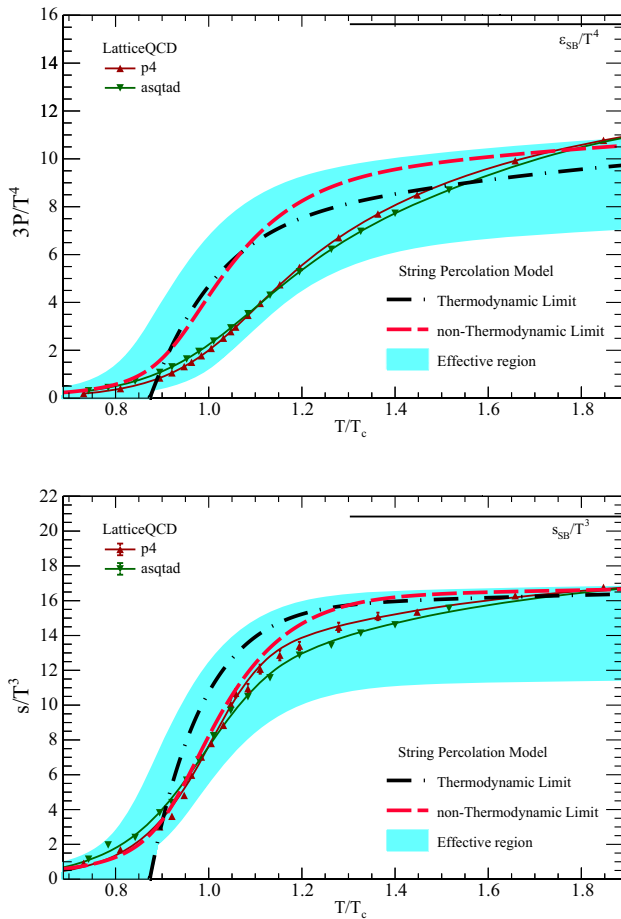


FIG. 5. Behavior of the (upper figure) pressure over T^4 and (lower figure) entropy density over T^3 against T/T_c , for TL (black dotted-dashed lines) and nonTL (red dashed lines) cases; we show the effective estimate region in the blue area. In both figures, the comparison with lattice QCD results p4 (maroon triangles) and asqtad (green triangles) actions with their respective parametrization (continuum lines) [65] are included.

VII. BULK VISCOSITY

The effects of bulk viscosity are known to be very small, which, in most of the high energy collisions, were neglected due to the thermalization of the system. However, great attempts have been made to obtain their value from nuclear collisions from RHIC to LHC [10,11].

Bulk viscosity corresponds to the resistance to the expansion of the fluid. The radial components seem damped due to the nonzero effect of bulk viscous pressure affecting the energy density profile of the created medium and converting it into pressure gradients changing the speed of sound c_s^2 [63]. This effect is related to the small perturbations produced in the medium formed [63], such as vibrations and rotations of the medium components. In the SPM framework, these effects correspond to the fluctuations of string properties (color field, string tension, etc). To determine the bulk viscosity, we calculate the speed of sound, which is given by a thermodynamic relation [64]:

$$c_s^2 = \left(\frac{\partial P}{\partial \varepsilon} \right)_s = s \left(\frac{\partial T}{\partial \varepsilon} \right)_s = -\frac{sT}{2\zeta F_s} \cdot \frac{dF_s}{d\xi}. \quad (17)$$

From Eqs. (6) and (7), it is simple to obtain $dF_s/d\xi$ of Eq. (17). In Fig. 6, we compute the effective region of c_s^2 . $F_s(\xi)$ gives a different behavior from what was previously reported in [5,6,9,63] and shows deviations from the results reported for elliptical geometry [19] that are all below our parametrization.

Specifically, we observed a large deviation from TL in the region below the critical temperature, showing a “dip-and-bump” effect; this behavior is in agreement with other phenomenological models [92] and goes accordingly with

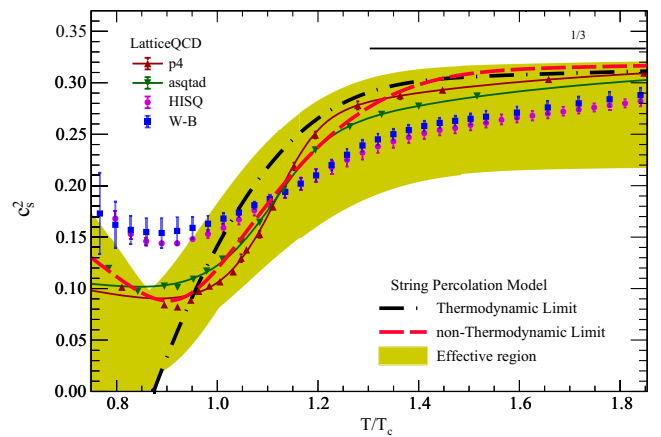


FIG. 6. Dependence of speed of sound squared with T/T_c calculated in the SPM framework using Eq. (17); the effective estimate region (golden area), the nonTL (red dashed line), and TL (black dotted-dashed line) limits are shown. The lattice QCD results from W-B (blue squares) [90], the magenta circles are the HISQ action extrapolated results from the HotQCD Collaboration [91] p4 (maroon triangles), and asqtad (green triangle) [65] actions from HotQCD collaboration are compared.

those reported from the lattice QCD 2 + 1 flavor staggered fermion actions p4 and asqtad from [65], the stout-link improved staggered fermion action from Wuppertal-Budapest Collaboration [90], and the highly improved staggered quark action from HotQCD Collaboration [91].

The first approximation of bulk viscosity over entropy density ζ/s of the simplest kinetic model in classical statistics with relaxation time approximation is given by [93]:

$$\frac{\zeta}{s} = 15 \frac{\eta}{s} \left(\frac{1}{3} - c_s^2 \right)^2, \quad (18)$$

which describes the bulk viscosity coefficient in terms of shear viscosity and speed of sound calculated in the SPM framework. The result of this approach using $F(\xi)$ and $F_s(\xi)$ is shown in dashed lines of Fig. 7. This approximation exhibits a monotonically decreasing behavior.

As a second approach, we use the results reported and verified in [95–100] of the projection operator approach to obtain the microscopic formulas for the transport coefficients in causal dissipative relativistic fluid dynamics (CDRF), in terms of the SPM observables T , s , Δ , c_s . The reported microscopic formula of the bulk viscosity ζ with its respective relaxation time τ_{Π} of CDRF is given by [95–101]:

$$\frac{\zeta}{s} = \left(\frac{1}{3} - c_s^2 \right) \tau_{\Pi} T - \frac{2\tau_{\Pi} T^4}{9s} \Delta, \quad (19)$$

where τ_{Π} is considered of the order of a fermi, and the fraction $2/9$ has to do with the number of fermionic degrees of freedom.

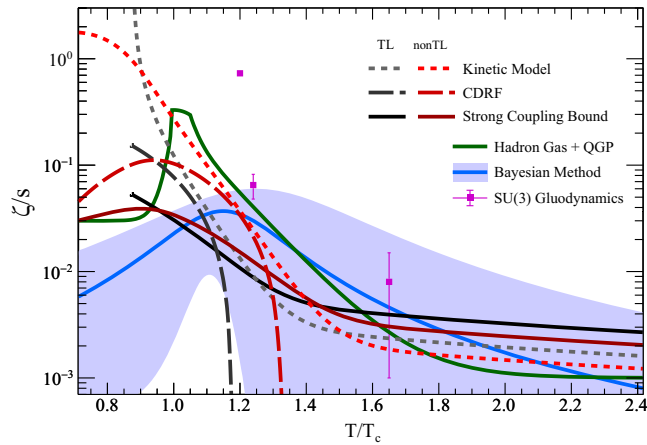


FIG. 7. Bulk viscosity over entropy density as a function of T/T_c from the kinetic model Eq. (18) (dotted lines), the CDRF formalism Eq. (19) (dashed lines), and the holographic limit using Eq. (20) (continuum lines) calculated in the SPM framework are shown; distinguish TL in gray scale lines and nonTL in red lines. The Bayesian method results [15] (blue region), the parametrization of Hadron Gas to QGP (continuum green line), and the SU(3) gauge theory calculations [94] are included.

The results of Eq. (19) in TL and nonTL are shown in Fig. 7 labeled as CDRF in which there are differences in their behaviors, and shifts in their vanishing points are shown.

On the other hand, in [17] is conjectured a lower limit on bulk viscosity of strongly coupled gauge theory plasmas as:

$$\frac{\zeta}{s} \geq 2 \left(\frac{1}{3} - c_s^2 \right) \frac{\eta}{s} \geq \frac{1}{2\pi} \left(\frac{1}{3} - c_s^2 \right), \quad (20)$$

considering $\eta/s \geq 1/(4\pi)$ [16], which is shown in solid black (TL) and red (nonTL) lines in Fig. 7.

Figure 7 includes the results of ζ/s reported from viscous relativistic hydrodynamics Bayesian method [15], which is near the holographic limit [17] and CDRF calculations in the SPM framework.

We compare our results of ζ/s with the hadron resonance gas model, which incorporates all identified particles and resonances with masses below 2 GeV, along with a density of Hagedorn states that increases exponentially for masses exceeding 2 GeV [102], and the continuum parametrization of the LQCD equation of state results of ζ/s of hot quark-gluon matter in the presence of light quarks [103], as presented in [104,105]. These models show a similar behavior to the kinetic model considered in the SPM ($T > T_c$ region). Also, the lattice gluodynamics calculation in SU(3) gauge theory [94] shows a scaled same dependence.

In Table I, we present the maximum values of ζ/s for the kinetic theory, CDRF formalism, and conjectured bound with its respective T/T_c value for TL and nonTL. We can observe that in all cases, ζ/s reaches its maximum value below the critical temperature, and the TL goes much higher than nonTL, reaching its maximum value. For the CDRF formalism, it is reached just 73.54% of the TL. For the lower conjectured bound, it is 72.97%, and for the case of the simplest kinetic model, we see a discrepancy in the values around 0.0052%, because the value of c_s^2 for TL vanishes at $T/T_c = 0.873553$; Eq. (18) gives the same tendency as shear viscosity over entropy density in TL.

In Fig. 8, we show the interplay between shear and bulk viscosity given by the ratio ζ/η computed in the SPM framework, where we can observe a maximum value around the critical temperature region in all cases. For the case of the kinetic model, the ζ/η ratio shows its

TABLE I. Results of the maximum value of bulk viscosity over entropy density for different approaches in TL and in our parametrization (nonTL).

	TL		nonTL	
	ζ/s (Max)	T/T_c	ζ/s (Max)	T/T_c
Kinetic	35132.6	0.873553	1.84112	0.146509
CDRF	0.152694	0.873553	0.111427	0.940129
Bound	0.0530515	0.873553	0.0390168	0.903653

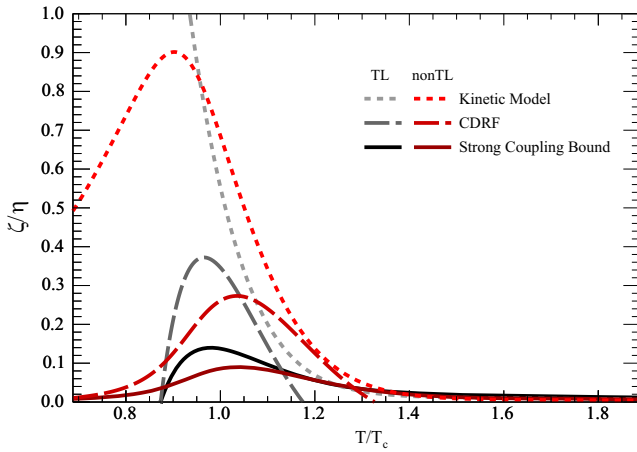


FIG. 8. The results of the bulk-shear viscosity ratio against T/T_c from the kinetic theory (dotted lines), CDRF (dashed lines) and the gauge theory plasma at strong coupling limit (continuum lines) [17] calculated in the SPM framework. Distinguish TL in gray lines and nonTL in red lines.

maximum value in $T < T_c$ for TL and nonTL scenarios, and for the CDRF formalism, we can see a change in the slope in the region just below $T = T_c$ for the TL case, and for nonTL right before $T = T_c$.

VIII. CONCLUSIONS

We have computed the η/s and ζ/s ratios by proposing a global parametrization for the SPM color reduction factor, which considers the small-bounded effects in the geometrical phase transition at the nonthermodynamic limit for $\mu_B = 0$. Our description highlights the differences in the physics behind both TL and nonTL cases discussed in the framework of the SPM for the QCD matter formed in pp and AA collisions at LHC energies.

The ratio η/s is estimated in a simplified kinetic formulation of an ideal gas of partons. The results on this coefficient show different minimum values in TL and nonTL, within the region $T_c < T < 1.23T_c$. The first implication related to the nonTL case reveals that a phase transition must occur at higher temperatures since a shift in the inflection point is found. Additionally, the medium effects that constrains particle movement are less pronounced on this limit, as can be seen in Fig. 3.

The behavior of the speed of sound shows that it does not vanish at low temperatures (Fig. 6). This is important since

c_s^2 acquires relevance in the computation of ζ/s , making its contribution non-neglectable.

For the estimation of ζ/s , we used two formalisms and compared them to a conjectured strong coupling bound. By using the CDRF on the SPM, we found that ζ/s vanishes at $T/T_c = 1.17$ for TL and at $T/T_c = 1.32$ for nonTL, as shown in Fig. 7. On the other hand, the implementation of the simplest kinetic model guides ζ/s to reach higher values before critical temperature, as summarized in Table I. Both formalisms are above the strong coupling bound for $T/T_c < 1.1$, where the maximum values are reached. Hence, the contribution of ζ becomes relevant in this region, implying that there is a strong effect driven by the fluctuations of the string properties, such as the color field, as well as the string tension. In addition, the ratio ζ/η for nonTL scenarios shows a shift of the maximum point, which is reached at higher temperatures. This implies that nonTL requires a higher temperature in order to reach phase transition due to the fluctuations coming from the bulk contributions (Fig. 8).

It is important to acknowledge certain limitations in our estimations of transport coefficients. First, our approach assumes that a cluster is locally in equilibrium in the initial state, which is crucial for the validity of Eq. (15). However, deviations from local equilibrium, especially in the early stages of high-energy collisions, could impact the accuracy of our estimations.

Our results show a clear difference in the behavior of the observables that take into account the finite size effects with respect to those that are predicted in the thermodynamic limit, showing that the fluctuations of the initial state have a qualitative relevance in the estimation of the coefficients that characterize the medium formed in small collisions systems.

While our study provides valuable insights into the behavior of transport coefficients in small collision systems within the framework of the string percolation model, one should remain mindful of these limitations when interpreting and applying our results.

ACKNOWLEDGMENTS

We thank CONAHCyT-México for supporting this work under the Project Nos. CF-2019/2042 and A1-S-26507. On the other hand, J. R. A. G. and P. F. thank CONAHCyT-México for the graduate fellowships 645654 and 848955, respectively.

[1] I. Bautista, J. D. de Deus, and C. Pajares, Elliptic flow at RHIC and LHC in the string percolation approach, *Eur. Phys. J. C* **72**, 2038 (2012).

[2] I. Bautista, C. Pajares, J. G. Milhano, and J. Dias de Deus, Rapidity dependence of particle densities in pp and AA collisions, *Phys. Rev. C* **86**, 034909 (2012).

- [3] I. Bautista, J. Dias de Deus, and C. Pajares, String percolation and the first LHC data, *Acta Phys. Pol. B Proc. Suppl.* **6**, 165 (2013).
- [4] C. Andrés, M. Braun, and C. Pajares, Energy loss as the origin of a universal scaling law of the elliptic flow, *Eur. Phys. J. A* **53**, 41 (2017).
- [5] B. K. Srivastava, Percolation and deconfinement, *Nucl. Phys.* **A862-863**, 132 (2011).
- [6] R. P. Scharenberg, B. K. Srivastava, and A. S. Hirsch, Percolation of color sources and the equation of state of QGP in central Au–Au collisions at $\sqrt{s_{NN}} = 200$ GeV, *Eur. Phys. J. C* **71**, 1510 (2011).
- [7] J. E. Ramírez, B. Díaz, and C. Pajares, Interacting color strings as the origin of the liquid behavior of the quark-gluon plasma, *Phys. Rev. D* **103**, 094029 (2021).
- [8] M. A. Braun and C. Pajares, Implications of color-string percolation on multiplicities, correlations, and the transverse momentum, *Eur. Phys. J. C* **16**, 349 (2000).
- [9] M. A. Braun, J. Dias de Deus, A. S. Hirsch, C. Pajares, and R. P. Scharenberg, B. K. Srivastava, De-confinement and clustering of color sources in nuclear collisions, *Phys. Rep.* **599**, 1 (2015).
- [10] V. Roy and A. K. Chaudhuri, Bulk viscosity in heavy ion collision, [arXiv:1201.4230](https://arxiv.org/abs/1201.4230).
- [11] J. E. Parkkila, A. Onnerstad, and D. J. Kim, Bayesian estimation of the specific shear and bulk viscosity of the quark-gluon plasma with additional flow harmonic observables, *Phys. Rev. C* **104**, 054904 (2021).
- [12] D. Everett *et al.*, Multisystem Bayesian constraints on the transport coefficients of QCD matter, *Phys. Rev. C* **103**, 054904 (2021).
- [13] H. Niemi, K. J. Eskola, and R. Paatelainen, Event-by-event fluctuations in a perturbative QCD + saturation + hydrodynamics model: Determining QCD matter shear viscosity in ultrarelativistic heavy-ion collisions, *Phys. Rev. C* **93**, 024907 (2016).
- [14] H. Niemi, K. J. Eskola, R. Paatelainen, and K. Tuominen, Predictions for 5.023 TeV Pb + Pb collisions at the CERN Large Hadron Collider, *Phys. Rev. C* **93**, 014912 (2016).
- [15] J. E. Bernhard, J. S. Moreland, and S. A. Bass, Bayesian estimation of the specific shear and bulk viscosity of quark-gluon plasma, *Nat. Phys.* **15**, 1113 (2019).
- [16] G. Policastro, D. T. Son, and A. O. Starinets, The Shear viscosity of strongly coupled $N = 4$ supersymmetric Yang-Mills plasma, *Phys. Rev. Lett.* **87**, 081601 (2001).
- [17] A. Buchel, Bulk viscosity of gauge theory plasma at strong coupling, *Phys. Lett. B* **663**, 286 (2008).
- [18] J. E. Ramírez, A. Fernández Téllez, and I. Bautista, String percolation threshold for elliptically bounded systems, *Physica (Amsterdam)* **488A**, 8 (2017).
- [19] J. E. Ramírez and C. Pajares, Area covered by disks in small-bounded continuum percolating systems: An application to the string percolation model, *Phys. Rev. E* **100**, 022123 (2019).
- [20] R. Bala, I. Bautista, J. Bielikova, and A. Ortiz, Heavy-ion physics at the LHC: Review of Run I results, *Int. J. Mod. Phys. E* **25**, 1642006 (2016).
- [21] C. Loizides, Experimental overview on small collision systems at the LHC, *Nucl. Phys.* **A956**, 200 (2016).
- [22] D. Stauffer, Scaling theory of percolation clusters, *Phys. Rep.* **54**, 1 (1979).
- [23] S. Kirkpatrick, Percolation and conduction, *Rev. Mod. Phys.* **45**, 574 (1973).
- [24] S. R. Broadbent and J. M. Hammersley, Percolation processes. 1. Crystals and mazes, *Proc. Cambridge Philos. Soc.* **53**, 629 (1957).
- [25] N. S. Amelin, M. A. Braun, and C. Pajares, Multiple production in the Monte Carlo string fusion model, *Phys. Lett. B* **306**, 312 (1993).
- [26] I. Bautista, C. Pajares, and J. E. Ramírez, String percolation in aa and p + p collisions, *Rev. Mex. Fis.* **65**, 197 (2019).
- [27] I. Bautista, A. F. Téllez, and P. Ghosh, Indication of change of phase in high-multiplicity proton-proton events at LHC in string percolation model, *Phys. Rev. D* **92**, 071504 (2015).
- [28] A. Rodrigues, R. Ugoccioni, and J. Dias de Deus, Percolation approach to phase transitions in high-energy nuclear collisions, *Phys. Lett. B* **458**, 402 (1999).
- [29] C. Albajar *et al.*, A study of the general characteristics of $p\bar{p}$ collisions at $\sqrt{s} = 0.2$ -TeV to 0.9-TeV, *Nucl. Phys.* **B335**, 261 (1990).
- [30] G. J. Alner *et al.*, UA5: A general study of proton-antiproton physics at $\sqrt{s} = 546$ -GeV, *Phys. Rep.* **154**, 247 (1987).
- [31] B. I. Abelev *et al.*, Systematic measurements of identified particle spectra in pp , d^+ Au and Au + Au collisions from STAR, *Phys. Rev. C* **79**, 034909 (2009).
- [32] CDF Collaboration, Pseudorapidity distributions of charged particles produced in $\bar{p}p$ interactions at $\sqrt{s} = 630$ GeV and 1800 GeV, *Phys. Rev. D* **41**, 2330(R) (1990).
- [33] K. Aamodt *et al.*, Charged-particle multiplicity measurement in proton-proton collisions at $\sqrt{s} = 0.9$ and 2.36 TeV with ALICE at LHC, *Eur. Phys. J. C* **68**, 89 (2010).
- [34] V. Khachatryan *et al.*, Transverse momentum and pseudorapidity distributions of charged hadrons in pp collisions at $\sqrt{s} = 0.9$ and 2.36 TeV, *J. High Energy Phys.* **02** (2010) 041.
- [35] V. Khachatryan *et al.*, Transverse-momentum and pseudorapidity distributions of charged hadrons in pp collisions at $\sqrt{s} = 7$ TeV, *Phys. Rev. Lett.* **105**, 022002 (2010).
- [36] J. Adam *et al.*, Pseudorapidity and transverse-momentum distributions of charged particles in proton-proton collisions at $\sqrt{s} = 13$ TeV, *Phys. Lett. B* **753**, 319 (2016).
- [37] V. Khachatryan *et al.*, Pseudorapidity distribution of charged hadrons in proton-proton collisions at $\sqrt{s} = 13$ TeV, *Phys. Lett. B* **751**, 143 (2015).
- [38] A. Bialas, Fluctuations of string tension and transverse mass distribution, *Phys. Lett. B* **466**, 301 (1999).
- [39] A. Di Giacomo and H. Panagopoulos, Field strength correlations in the QCD vacuum, *Phys. Lett. B* **285**, 133 (1992).
- [40] A. Di Giacomo, Extracting physics from lattice artifacts, *Acta Phys. Pol. B* **25**, 227 (1994).
- [41] G. S. Bali, K. Schilling, and C. Schlichter, Observing long color flux tubes in SU(2) lattice gauge theory, *Phys. Rev. D* **51**, 5165 (1995).

- [42] J. Dias de Deus and C. Pajares, Percolation of color sources and critical temperature, *Phys. Lett. B* **642**, 455 (2006).
- [43] L. J. Gutay, A. S. Hirsch, C. Pajares, R. P. Scharenberg, and B. K. Srivastava, De-confinement in small systems: Clustering of color sources in high multiplicity $\bar{p}p$ collisions at $\sqrt{s} = 1.8$ TeV, *Int. J. Mod. Phys. E* **24**, 1550101 (2015).
- [44] R. P. Scharenberg, B. K. Srivastava, and C. Pajares, Exploring the initial stage of high multiplicity proton-proton collisions by determining the initial temperature of the quark-gluon plasma, *Phys. Rev. D* **100**, 114040 (2019).
- [45] A. N. Mishra, G. Paić, C. Pajares, R. P. Scharenberg, and B. K. Srivastava, Exploring the QGP phase above the deconfinement temperature in pp and $A-A$ collisions at LHC energies, [arXiv:2202.12274](https://arxiv.org/abs/2202.12274).
- [46] I. Bautista Guzman, R. Alvarado, and P. Fierro, Collectivity in pPb and pp collisions with the string percolation model, *Proc. Sci. ICHEP2016* (2017) 1152.
- [47] J. C. T. García, D. R. Herrera, J. E. Ramírez, A. Fernández Téllez, and C. Pajares, Percolation leads to finite-size effects on the transition temperature and center-of-mass energy required for quark-gluon plasma formation, *Phys. Rev. D* **106**, L031503 (2022).
- [48] R. P. Scharenberg, B. K. Srivastava, A. S. Hirsch, and C. Pajares, Hot dense matter: Deconfinement and clustering of color sources in nuclear collisions, *Universe* **4**, 96 (2018).
- [49] STAR Collaboration, Transverse momentum and collision energy dependence of high $p(T)$ hadron suppression in Au + Au collisions at ultrarelativistic energies, *Phys. Rev. Lett.* **91**, 172302 (2003).
- [50] ALICE Collaboration, Transverse momentum spectra and nuclear modification factors of charged particles in pp, p-Pb and Pb-Pb collisions at the LHC, *J. High Energy Phys.* **11** (2018) 013.
- [51] ALICE Collaboration, Energy dependence of the transverse momentum distributions of charged particles in pp collisions measured by ALICE, *Eur. Phys. J. C* **73**, 2662 (2013).
- [52] ALICE Collaboration, Charged-particle production as a function of multiplicity and transverse spherocity in pp collisions at $\sqrt{s} = 5.02$ and 13 TeV, *Eur. Phys. J. C* **79**, 857 (2019).
- [53] ATLAS Collaboration, Charged-particle distributions in $\sqrt{s} = 13$ TeV pp interactions measured with the ATLAS detector at the LHC, *Phys. Lett. B* **758**, 67 (2016).
- [54] S. Chatrchyan *et al.*, Study of the inclusive production of charged pions, kaons, and protons in pp collisions at $\sqrt{s} = 0.9, 2.76,$ and 7 TeV, *Eur. Phys. J. C* **72**, 2164 (2012).
- [55] S. Chatrchyan *et al.*, Study of the production of charged pions, kaons, and protons in pPb collisions at $\sqrt{s_{NN}} = 5.02$ TeV, *Eur. Phys. J. C* **74**, 2847 (2014).
- [56] A. M. Sirunyan *et al.*, Measurement of charged pion, kaon, and proton production in proton-proton collisions at $\sqrt{s} = 13$ TeV, *Phys. Rev. D* **96**, 112003 (2017).
- [57] J. S. Schwinger, Gauge invariance and mass. 2., *Phys. Rev.* **128**, 2425 (1962).
- [58] S. Mertens and C. Moore, Continuum percolation thresholds in two dimensions, *Phys. Rev. E* **86**, 061109 (2012).
- [59] J. Dias de Deus, A. S. Hirsch, C. Pajares, R. P. Scharenberg, and B. K. Srivastava, Transport coefficient to trace anomaly in the clustering of color sources approach, *Phys. Rev. C* **93**, 024915 (2016).
- [60] A. Bazavov *et al.*, Chiral and deconfinement aspects of the qcd transition, *Phys. Rev. D* **85**, 054503 (2012).
- [61] R. Hagedorn, Multiplicities, p_T distributions and the expected hadron \rightarrow quark—gluon phase transition, *Riv. Nuovo Cimento* **6N10**, 1 (1983).
- [62] J. Dias de Deus, A. S. Hirsch, C. Pajares, R. P. Scharenberg, and B. K. Srivastava, Clustering of color sources and the shear viscosity of the QGP in heavy ion collisions at RHIC and LHC energies, *Eur. Phys. J. C* **72**, 2123 (2012).
- [63] P. Sahoo, S. K. Tiwari, S. De, R. Sahoo, R. P. Scharenberg, and B. K. Srivastava, Thermodynamic and transport properties in Au + Au collisions at RHIC energies from the clustering of color strings, *Mod. Phys. Lett. A* **34**, 1950034 (2019).
- [64] J. D. Bjorken, Highly relativistic nucleus-nucleus collisions: The central rapidity region, *Phys. Rev. D* **27**, 140 (1983).
- [65] A. Bazavov *et al.*, Equation of state and QCD transition at finite temperature, *Phys. Rev. D* **80**, 014504 (2009).
- [66] F. Karsch, Lattice results on QCD thermodynamics, *Nucl. Phys.* **A698**, 199 (2002).
- [67] K. Adcox *et al.*, Formation of dense partonic matter in relativistic nucleus-nucleus collisions at RHIC: Experimental evaluation by the PHENIX collaboration, *Nucl. Phys.* **A757**, 184 (2005).
- [68] B. B. Back *et al.*, The PHOBOS perspective on discoveries at RHIC, *Nucl. Phys.* **A757**, 28 (2005).
- [69] I. Arsene *et al.*, Quark gluon plasma and color glass condensate at RHIC? The perspective from the BRAHMS experiment, *Nucl. Phys.* **A757**, 1 (2005).
- [70] J. Adams *et al.*, Experimental and theoretical challenges in the search for the quark gluon plasma: The STAR Collaboration's critical assessment of the evidence from RHIC collisions, *Nucl. Phys.* **A757**, 102 (2005).
- [71] K. Aamodt *et al.*, Elliptic flow of charged particles in Pb-Pb collisions at 2.76 TeV, *Phys. Rev. Lett.* **105**, 252302 (2010).
- [72] S. Chatrchyan *et al.*, Measurement of the elliptic anisotropy of charged particles produced in PbPb collisions at $\sqrt{s_{NN}} = 2.76$ TeV, *Phys. Rev. C* **87**, 014902 (2013).
- [73] G. Aad *et al.*, Measurement of the pseudorapidity and transverse momentum dependence of the elliptic flow of charged particles in lead-lead collisions at $\sqrt{s_{NN}} = 2.76$ TeV with the ATLAS detector, *Phys. Lett. B* **707**, 330 (2012).
- [74] K. Aamodt *et al.*, Higher harmonic anisotropic flow measurements of charged particles in Pb-Pb collisions at $\sqrt{s_{NN}} = 2.76$ TeV, *Phys. Rev. Lett.* **107**, 032301 (2011).
- [75] S. Chatrchyan *et al.*, Studies of Azimuthal dihadron correlations in ultra-central PbPb collisions at $\sqrt{s_{NN}} = 2.76$ TeV, *J. High Energy Phys.* **02** (2014) 088.

- [76] V. Khachatryan *et al.*, Observation of long-range near-side angular correlations in proton-proton collisions at the LHC, *J. High Energy Phys.* **09** (2010) 091.
- [77] B. Abelev *et al.*, Long-range angular correlations on the near and away side in p -Pb collisions at $\sqrt{s_{NN}} = 5.02$ TeV, *Phys. Lett. B* **719**, 29 (2013).
- [78] S. Chatrchyan *et al.*, Observation of long-range near-side angular correlations in proton-lead collisions at the LHC, *Phys. Lett. B* **718**, 795 (2013).
- [79] V. Khachatryan *et al.*, Evidence for collectivity in pp collisions at the LHC, *Phys. Lett. B* **765**, 193 (2017).
- [80] M. Aaboud *et al.*, Measurement of multi-particle azimuthal correlations in pp , $p + \text{Pb}$ and low-multiplicity $\text{Pb} + \text{Pb}$ collisions with the ATLAS detector, *Eur. Phys. J. C* **77**, 428 (2017).
- [81] T. Hirano and M. Gyulassy, Perfect fluidity of the quark gluon plasma core as seen through its dissipative hadronic corona, *Nucl. Phys.* **A769**, 71 (2006).
- [82] M. Baker, P. Cea, V. Chelnokov, L. Cosmai, F. Cuteri, and A. Papa, The confining color field in SU(3) gauge theory, *Eur. Phys. J. C* **80**, 514 (2020).
- [83] H. B. Meyer, A calculation of the shear viscosity in SU(3) gluodynamics, *Phys. Rev. D* **76**, 101701 (2007).
- [84] M. Bluhm, B. Kampfer, and K. Redlich, Bulk and shear viscosities of the gluon plasma in a quasiparticle description, *Phys. Rev. C* **84**, 025201 (2011).
- [85] A. D. Gasbarro, Studies of conformal behavior in strongly interacting quantum field theories, Ph.D. thesis, Yale U., 2019.
- [86] K. I. Ishikawa, Y. Iwasaki, Y. Nakayama, and T. Yoshie, Conformal behavior in QCD, [arXiv:1304.4345](https://arxiv.org/abs/1304.4345).
- [87] M. Cheng *et al.*, Equation of state for physical quark masses, *Phys. Rev. D* **81**, 054504 (2010).
- [88] B. K. Srivastava, Percolation approach to initial stage effects in high energy collisions, *Nucl. Phys.* **A926**, 142 (2014).
- [89] T. Schäfer and D. Teaney, Nearly perfect fluidity: From cold atomic gases to hot quark gluon plasmas, *Rep. Prog. Phys.* **72**, 126001 (2009).
- [90] S. Borsányi, Z. Fodor, C. Hoelbling, S. D. Katz, S. Krieg, and K. K. Szabó, Full result for the qcd equation of state with $2 + 1$ flavors, *Phys. Lett. B* **730**, 99 (2014).
- [91] A. Bazavov *et al.*, Equation of state in $(2 + 1)$ -flavor QCD, *Phys. Rev. D* **90**, 094503 (2014).
- [92] W.-b. He, G.-y. Shao, X.-y. Gao, X.-r. Yang, and C.-l. Xie, Speed of sound in QCD matter, *Phys. Rev. D* **105**, 094024 (2022).
- [93] K. Dusling and T. Schäfer, Bulk viscosity, particle spectra and flow in heavy-ion collisions, *Phys. Rev. C* **85**, 044909 (2012).
- [94] H. B. Meyer, A calculation of the bulk viscosity in SU(3) gluodynamics, *Phys. Rev. Lett.* **100**, 162001 (2008).
- [95] T. Koide, Microscopic formula of transport coefficients for causal hydrodynamics, *Phys. Rev. E* **75**, 060103 (2007).
- [96] T. Koide and T. Kodama, Transport coefficients of non-Newtonian fluid and causal dissipative hydrodynamics, *Phys. Rev. E* **78**, 051107 (2008).
- [97] T. Koide, E. Nakano, and T. Kodama, Shear viscosity coefficient and relaxation time of causal dissipative hydrodynamics in QCD, *Phys. Rev. Lett.* **103**, 052301 (2009).
- [98] X.-G. Huang, T. Kodama, T. Koide, and D. H. Rischke, Bulk viscosity and relaxation time of causal dissipative relativistic fluid dynamics, *Phys. Rev. C* **83**, 024906 (2011).
- [99] G. S. Denicol, X.-G. Huang, T. Koide, and D. H. Rischke, Consistency of field-theoretical and kinetic calculations of viscous transport coefficients for a relativistic fluid, *Phys. Lett. B* **708**, 174 (2012).
- [100] T. Koide, Microscopic derivation of causal diffusion equation using projection operator method, *Phys. Rev. E* **72**, 026135 (2005).
- [101] X.-G. Huang and T. Koide, Shear viscosity, bulk viscosity and relaxation times of causal dissipative relativistic fluid-dynamics at finite temperature and chemical potential, *Nucl. Phys.* **A889**, 73 (2012).
- [102] J. Noronha-Hostler, J. Noronha, and C. Greiner, Transport coefficients of hadronic matter near $T(c)$, *Phys. Rev. Lett.* **103**, 172302 (2009).
- [103] F. Karsch, D. Kharzeev, and K. Tuchin, Universal properties of bulk viscosity near the QCD phase transition, *Phys. Lett. B* **663**, 217 (2008).
- [104] G. S. Denicol, T. Kodama, T. Koide, and P. Mota, Effect of bulk viscosity on Elliptic Flow near QCD phase transition, *Phys. Rev. C* **80**, 064901 (2009).
- [105] S. Ryu, J. F. Paquet, C. Shen, G. S. Denicol, B. Schenke, S. Jeon, and C. Gale, Importance of the bulk viscosity of QCD in ultrarelativistic heavy-ion collisions, *Phys. Rev. Lett.* **115**, 132301 (2015).